INVESTIGATING DRAINAGE RATE EFFECTS ON FRACTAL PATTERNS AND CAPILLARY FINGERING IN A REALISTIC GLASS MICROMODEL

Mohammad Nadafpour, Mohammad Reza Rasaei

Original scientific paper

Proper characterization of fluid displacement processes and mechanisms at pore scale is essential to understand and describe the displacement behaviour at larger core and reservoir scales. Detailed visual investigation of displacement phenomena is only realized using real-size glass micromodels similar to what we developed in this study. Different drainage rate experiments are performed with viscosity match fluids to observe flow patterns in a water-wet glass micromodel. Total saturation S_t, local saturations S_x, front fractal dimension D_f and surface fractal dimension D_s, are calculated from high resolution images of the tests and are used for the qualitative and quantitative evaluation of the processes. It is found that S_t and D_s follow increasing trends and D_f tracks a decreasing trend with capillary number. This is due to the more stable patterns and compact structures that are developed in the tests with higher injection rates. S_x curves, however, remained comparable for different capillary number tests due to the same network pattern used in all the experiments. Advanced fractal measures along with high resolution images of the experiments made it possible to precisely describe and investigate the displacement patterns and structures as they initiate and develop with time at different combinations of capillary and viscous forces most likely encountered in real reservoir conditions.

Keywords: *capillary number, drainage, micromodel, flow pattern, front fractal dimension, surface fractal dimension, total saturation, viscosity matched*

Istraživanje učinaka brzine drenaže na fraktalne uzorke i kapilarni fingering u realnom staklenom mikromodelu

Izvorni znanstveni članak

Ispravna karakterizacija postupaka i mehanizama istiskivanja fluida razmjera pora je od bitne važnosti za razumijevanje i opisivanje ponašanja pri istiskivanju kod većih mjera jezgre i rezervoara. Detaljno vizualno ispitivanje fenomena istiskivanja može se ostvariti jedino korištenjem staklenih mikromodela stvarnih dimenzija sličnih onom razvijenom u ovom radu. Provedena su razna ispitivanja brzine drenaže s fluidima iste viskoznosti u svrhu promatranja uzoraka toka u vodom ovlaženom staklenom mikromodelu. Potpuno zasićenje S_t, lokalna zasićenja S_x, prednja fraktalna dimenzija D_f i površinska fraktalna dimenzija D_s, izračunati su iz slika testova visoke rezolucije i upotrijebljeni za kvalitativnu i kvantitativnu procjenu postupaka. Ustanovljeno je da S_t i D_s prate trendove porasta, a staze D_f trend opadanja s kapilarnim brojem. To se događa zbog stabilnijih uzoraka i kompaktnih struktura koje se razvijaju u testovima s većim brzinama ubrizgavanja. Krivulje S_x su, međutim, ostale usporedive kod različitog broja kapilarnih testova zbog istog uzorka mreže primijenjenog u svim eksperimentima. Napredne fraktalne mjere zajedno sa slikama eksperimenata visoke rezolucije omogućile su da se precizno opišu i istraže uzorci i strukture istiskivanja kako se stvaraju i s vremenom razvijaju pri različitim kombinacijama kapilarnih i viskoznih sila na koje se najvjerojatnije nailazi u stvarnim uvjetima spremišta.

Ključne riječi: *čelna fraktalna dimenzija, drenaža, kapilarni broj mikromodel, odgovarajući viskozitet, potpuno zasićenje, površinska fraktalna dimenzija, uzorak toka*

1 Introduction

Investigation of multi-phase flow patterns in porous media is a subject of scientific study of subsurface processes of enhanced oil and gas recovery, geological carbon sequestration and non-aqueous phase liquid contamination of ground water. There is a rich literature on both drainage (wetting phase displacement by non-wetting phase) and imbibition (reverse of drainage) processes. Flow behavior in porous media is strongly affected by fluids properties (viscosity, density, and interfacial tension), rock properties (geometry and topology of pores, heterogeneity, and wettability) and flow rates [1]. By changing these parameters individually or together, a great variety of structures are observed, which makes the study of fluid flow in porous media a fascinating and complex challenge [2 ÷ 5]. Micromodels are used to visualize the pore scale multi-phase displacement phenomena [6]. Despite the fact that micromodels are 2D systems, pore scale processes observed by these systems provide valuable insights and implication for processes occurring at the continuum scale. The results obtained from these experiments help to develop more realistic models for future reservoir behaviour prediction. Two-dimensional micromodels are designed to artificially replicate porous media etched into materials such as silicon [5, 7], glass [8] and

polydimethylsiloxsan (PDMS)[9]. It is now possible to construct a wide variety of pore structures with realistic pore and throat size distributions.

The majority of two-phase displacement studies using micromodels have been conducted for imbibition process because of interest in enhanced oil recovery processes [10, 11]. Increased recent emphasis on subsurface injection of low viscosity supercritical CO_2 has renewed interest in pore scale research for drainage system which mostly originates from Lenormand et al. [1, 5, 6, 12].

Multi-phase displacement pattern in drainage processes is affected by three forces: viscous force of invading and defending fluids [2, 13] , capillary force due to the interfacial forces between them [14] and gravity force due to their density difference [15, 16]. Gravity force is diminished in horizontal systems. The remaining forces are described by two dimensionless numbers of viscosity ratio M, and capillary number Ca. Viscosity ratio M, is defined as the viscosity of the defending phase μ_d divided by that of the invading phase μ_i/$M = \mu_d/\mu_i$. Capillary number, Ca, presents the competition between capillary and viscous forces defined as $Ca = \mu \cdot u/(\sigma_{nw} \cos \theta)$ where μ is the maximum viscosity of the fluids, u is the velocity of the advancing fluid, σ_{nw} is the interfacial tension, and θ is the fluid-solid contact angle.

These forces specify the flow regimes and displacement structures that are developed in porous

media [5, 17]. Three major structures are defined as viscous fingering, stable displacement and capillary fingering [6, 13]. Viscous fingering happens when capillary number is high (the viscous force is dominant) or $M>1$ (defending phase viscosity is higher than that of the invading phase).This flow pattern is characterized by self-similar diffusion-limited-aggregation (DLA) model [17-20]. When capillary number is near to zero, viscous and gravity forces are negligible, and displacement is governed by capillary forces [19, 21].

When the fluid velocity in drainage processes approaches zero, uniform pressures are developed in the inlet and outlet regions of the porous medium. In this condition, pore size distribution controls the fluids movement and a capillary fingering pattern is developed, i.e. the non-wetting fluid pressure can only exceed entry capillary pressure of a large pore throat with a radius r: $p_c = 2\sigma_{nw}/r$. The non-wetting fluid then gently percolates into the larger pore throats with smaller capillary pressures. In this circumstance of slow drainage, the front motion is discontinuous but occurs in sudden bursts called Haines jumps [22]. Theoretical [23 ÷ 25] and experimental [24, 26] studies have confirmed this phenomenon in slow drainages. The modelling techniques of invasion percolation (IP) [21, 27] and invasion percolation with trapping (IPT) [28 ÷ 30] are used in these systems. It is worth to mention that these models are applicable to regions far from the injection wells where the viscous force is diminished due to small local flow velocity.

Two fractal dimensions are introduced to specify the disorder degree of the displacement front and the dispersion amount of displacing phase in the pore network. Front fractal dimension with the value of D_f=1,33 [31 ÷ 33] which seems to be very close to the fractal dimension of the external perimeter of the percolation cluster [3]. Surface fractal dimension(fractal dimension of entire fluid cluster) in large two dimensional flow systems with self-similar property of injected fluid has the value of D_s =1,82 [34, 25]; This is slightly lower than the critical value of the ordinary percolation theory, D_s=1,89 [36 ÷ 38]. Usually the value of theoretical percolation fractal dimension D_s=1,89, matches the observed results in smaller systems [3, 39]. In three dimensional systems, several experiments have been performed (40 ÷ 42). The mass fractal dimension found at small scale (between 2 and 2,6) is compatible with the D_m=2,5 found in three dimensional invasion percolation models (21).

Numerous experimental and numerical studies of drainage processes with different capillary numbers and viscosity ratios are performed. Viscosity matched fluids tests (M=1) are, however, rarely considered; the only study performed in glass beads [33] with very high porosity of 0,7 showed a front fractal dimension of D_f=1,33 which is confirmed with numerical results [43].

To our knowledge, viscosity matched drainage experiments on more realistic porous media, such as the glass micromodel we manufactured here, have not been conducted before. In order to make qualitative and quantitative description of the displacement patterns and the developed structures, advanced fractal measures along with high resolution images of each process are used.

The structure of the paper is as follows: the micromodel properties and experimental setup are described in the next section. Then, the tests procedures and the experiments we performed to investigate the flow rate effects on displacement patterns are presented. The results of the experiments and their analyses and evaluations are given later. The paper is then concluded with the summary section and mentioning the main findings of this study.

2 Micromodel and experimental setup
2.1 Micromodel properties

Micromodel is fabricated in borosilicate glass using standard nanolithography and wet etching technique [44, 45]. The micromodel consists of one inlet channel, connected to a pore network (Fig. 1(a)) and one outlet channel. The width of throats varies randomly from 25 μm to 75 μm; pores are 200 μm apart with constant sizes of 300 × 300 μm and porosity of 0,42. The model consists of 70 and 140 rows of throats respectively along and perpendicular to the average flow direction; thus a total number of 9800 throats was obtained. Fig. 2 shows the histogram of throat width. The average depth of the etched pore network is 37 μm (measured with DEKTAK profilometer), with the variation of ±3 μm due to the non-uniformity associated with the wet etching technique. It must be noted that wet etching of glass can result in walls with the angles of 10 ÷ 20°, and undercutting occurrence. The flow channels were sealed with a cover glass sheet. This glass has two drilled holes as flow inlet and outlet path. The constructed micromodel was then placed in two steel frames as a holder box to prevent any possible disjoint or misfit.
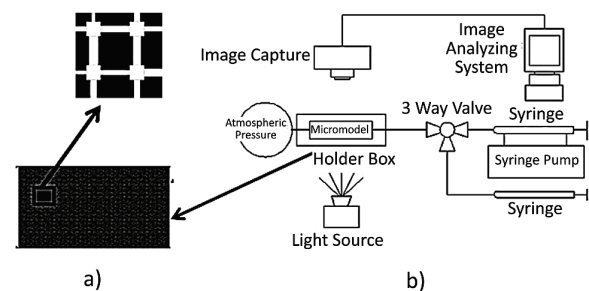

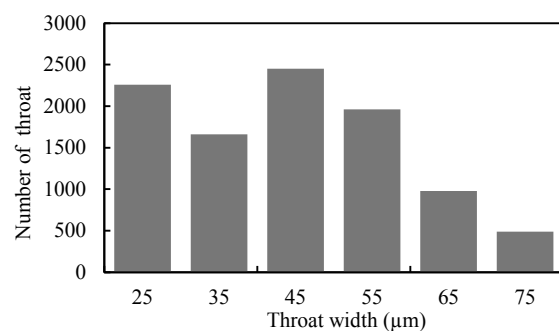**Figure 1** Schematic of the (a) network pattern, (b) experimental setup

Figure 2 The number distribution of throat versus throat width ranging from 25 μm to 75 μm

2.2 Experimental setup

Schematic diagram of the experimental setup is shown in Fig. 1(b). A Nexus 6000 syringe pump was used

which can operate in a wide range of injection rates between 0,00001 μl/min and 200 μl/min. A three-way valve was placed at the entrance of the model to make it possible to saturate the model while it was connected to the pump.

The wetting nature of the substrate was determined by measurement of contact angle between the glass and the fluid phases. This was performed by sessile-drop method and contact angle of $\theta=43°$ was obtained. Oil-water interfacial tension of $52,5\times10^{-5}$ N/cm was also measured by pendant-drop method. All the experiments were performed at constant laboratory temperature of 24 °C to keep a fixed viscosity ratio of one during the tests.

3   Tests procedure

At the start of each test, the cleaned micromodel was saturated with water, and n-Decane was then injected as non-wetting phase. Several experiments at different injection rates between 5 μl/h to 1000 μl/h were conducted to study the developed drainage patterns and displacement structures. After each experiment, the micromodel was thoroughly cleaned using a rigorous cleaning procedure in the following order: acetone, deionized water, and piranha mixture (a 1:1:5 solution of ammonium (NH_3), hydrogen peroxide (H_2O_2) and deionized water).

High resolution pictures from top of the micromodel were taken while it was illuminated from below with UV light. A 21 megapixel Canon-5D digital camera equipped with a 65MPE macro lens was used for this purpose. The images with resolution of 5616×3744 pixels cover a physical area of $43 \times 28,66$ mm^2 of the micromodel. The physical length of each pixel is around 7,6 μm so the number of pixels per throats width varied from 4 to 11 pixels

(a)   (b)
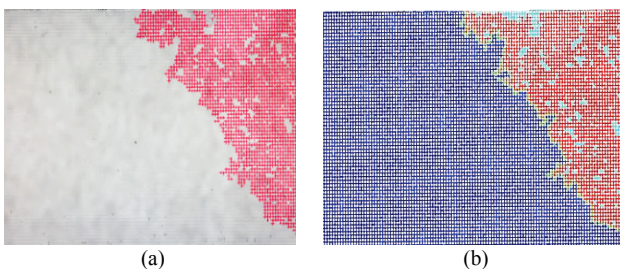
Figure 3 Image processing analysis: (a) Real image; (b) Processed image (defending fluid in blue, front in green, invading fluid in red, and unsweep defending fluid in light blue).

Special image processing software was developed to analyse the pictures. All image pixels were analysed to produce histograms of Red, Green, Blue, Hue, Saturation, and Brightness, which describe differences in colours. Characterization of these histograms makes it possible to distinguish the oil and the water phases by converting the coloured pictures to binary coloured images of these phases. According to the threshold specified above, all pixels were converted to blue (water) and the rest were converted to red (oil). Since the injected water and grains are isochromatic, a covering mask was designed to distinguish the grains and blacken them in the analysis step. Once the flow pattern was characterized by image analysis routine, total and local network saturations, front

fractal dimension and surface fractal dimension were calculated. A typical flow pattern and the analysed image are shown in Fig. 3. At very low injection rate of 5 μl/h (Ca=2,73E−8) capillary fingering is expected. The front (green) between the invading (red) and defending fluids (blue) appears as a complicated path connecting the left and right boundaries of the lattice. The inundation structure and the trapping, both indicative of capillary fingering, are clearly evident in this picture

Detailed image analysis was performed to calculate various statistical descriptions including: total network saturation S_t, local saturation S_x, front fractal dimension D_f, and surface fractal dimension D_s. Fig. 4 shows typical trends of these parameters as the displacement front proceeds to the outlet boundary of the micromodel. As shown in Fig. 4(a-2) and 4(b), total network saturation is defined as $S_t = N_{inv}/N_{tot}$ where N_{inv} and N_{tot} are the number of pixels of the invading phase and the total number of the pore space pixels of the network respectively. The local saturation shown in Fig. 4 (a-2) and (c) is defined as $S_x = N_{(x)inv}/N_{(x)tot}$ where x is the column index, running between 1 to 1180 from the inlet to the outlet of the micromodel. Due to the large number of pixels, we considered each column index to represent 8 consecutive adjacent columns of the pixels. $N_{(x)inv}$ and $N_{(x)tot}$ are the number of pixels of invading phase and the total number of pore pixels for a given x, respectively.

In this analysis, the fractal dimension D of the images was used to quantify their structural changes with time. The fractal dimension is a measure of how the invading phase 'takes up space' within the microfluidic pore network [18]. Generally, mathematical and natural fractals are shapes whose irregularity and division neither tend to vanish, nor fluctuate up and down, but remain essentially unchanged as one zoom.

Box counting method was used to calculate fractal dimension of the flow pattern and invading phase front. The basic procedure is to systematically lay a series of grids of decreasing size (the boxes) over the image and record the data (the counting) for each successive calibre. Counting is usually a matter of recording how many boxes in each grid belong to the invading phase in the image. This is defined as follow:

$$D = \lim_{\delta \to 0} \frac{\lg N(\delta)}{-\lg \delta}, \tag{1}$$

where $N(\delta)$ is the number of boxes of size δ which is needed to cover the flow image. In our experiments, two types of fractal dimensions for each sequence of images is calculated: (a) front fractal dimensions, and (b) surface fractal dimension as shown in Figs. 4(a-3) and 4(d).

4   Results and discussion

As mentioned before, drainage experiments at different injection rates were conducted to investigate the capillary fingering characteristics, i.e. trapping and front fingering structure. Capillary number in these experiments was changed over two orders of magnitude as presented in Tab. 1. All displacement experiments were performed under three replicates for each capillary

number. Bouncy effect is likely to be negligible in these experiments because of the horizontal configuration and limited vertical depth of the micromodel. Each experiment was run until breakthrough time of the injected fluid. Breakthrough time was calculated as the time at which the fluid interface reaches the outlet.

Breakthrough time followed a rather sharp decreasing trend with capillary number in the conducted tests (Fig. 5). This is an indication of more stable displacement as viscous force becomes more important. We will come back to this shortly when we consider the saturation patterns and related fractal dimension in the next sections.

4.1 Total saturation

Total saturation S_t, is the cumulative pore volume fraction of the network occupied by the invading phase. For proper comparison of different tests, a dimensionless time, t_D, (the ratio of real time to breakthrough time, t_{bt}) was used.

All the tests were analysed till their dimensionless time value reached to one. Linear trend of S_t with t_D was expected due to the existence of incompressible fluids as observed in Fig. 6. Piston-like stable displacement with low trapping appeared as a high slope line; the slope was decreased due to the dominant displacement configurations of fingering and trapping phenomena. It can be inferred from this figure that the front instability and fingering-type behaviour decreased with injection rate since the tests with higher injection rate showed a higher slope, i.e. faster increase of S_t with t_D.

Table 1 Injection rates and breakthrough times of one series of drainage experiments

Test	Injection rate ($\mu l/h$)	Capillary number	Breakthrough time (s)
1	5	2,73E−08	11520
2	20	1,09E−07	3694
3	50	2,73E−07	1444
4	75	4,10E−07	1092
5	100	5,46E−07	916
6	200	1,09E−06	826
7	300	1,62E−06	630
8	400	2,18E−06	480
9	500	2,73E−06	270
10	600	3,25E−06	191
11	700	3,82E−06	150
12	800	4,33E−06	140
13	900	4,87E−06	126
14	1000	5,41E−06	94

At low capillary number, the capillary force controls the movement of viscosity matched fluids through the largest throats in any direction; the direction perpendicular to the average flow path or even into the pores in the backward direction. The capillary fingers of invaded fluid are narrower than the fjord of the displaced fluid, as can be seen in Fig. 3. In addition, local trapping reduces the effective mobility of the displacing fluid which may just be interpreted as an increase in effective dynamic viscosity. Thus we are effectively dealing with a more viscous liquid displacing a less viscose liquid, which leads to stable front by increasing capillary number.
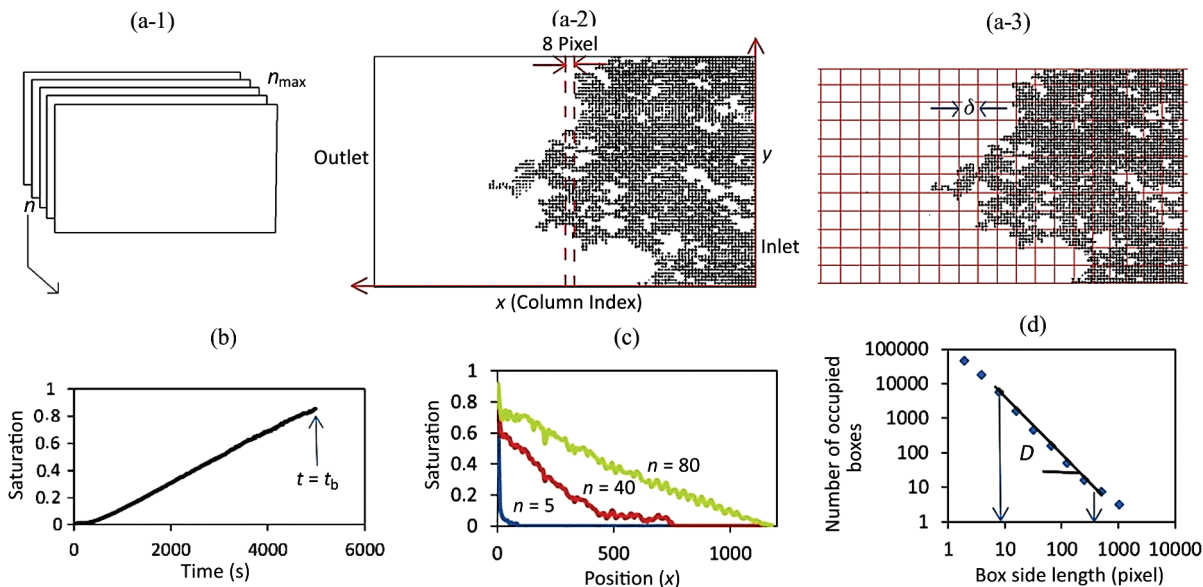
Figure 4 Image analysis procedure: (a-1) Series of pore network images; (a-2) S_x calculation in each column; (a-3) Surface fractal dimension analysis (D_s); (b) S_t as a function of time; (c) Saturation profiles for three selected time step; (d) Calculation of D_f.

With this argument, we expected to observe a higher S_t at breakthrough time at higher injection rate tests. This is actually the case as we presented in Fig. 7. The slowest drainage test resulted in the lowest S_t (i.e. most unstable displacement pattern) and the fastest drainage test corresponded to the highest S_t (i.e. most stable displacement pattern) at their respective breakthrough times.
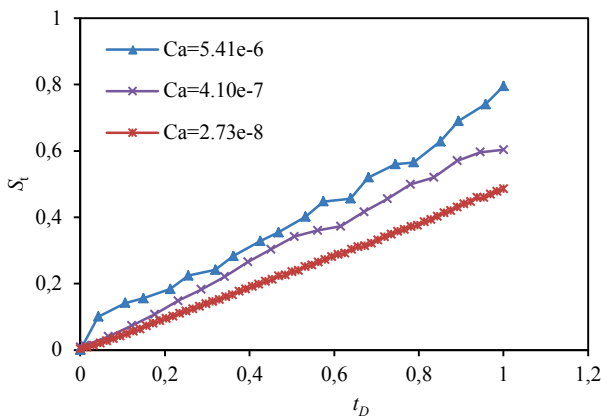
4.2 Local saturation

Local saturation S_x, is the non-wetting phase saturation of the column index x, at the instantaneous moment of time. This is related to two-phase flow dynamics in porous media. Local saturation profiles at different times are illustrated in Fig. 8 for a specified capillary number Ca=2,73E−8. In this figure the first curve corresponds to the time t=0 of oil invasion and the

last curve belongs to the breakthrough time. It should be noted that in each experiment the image acquisition time interval maintained constant.

Due to the trapping and bypassing of the wetting phase, the local saturation never reaches its maximum value of S_x=1, as it is evident in Fig. 8. Non-uniform distribution of the trapped wetting phase in this figure indicates the heterogeneous nature of the constructed pore network pattern. Fig. 9 shows S_x values from the inlet to the outlet columns for three tests with different injection rates at their breakthrough time.
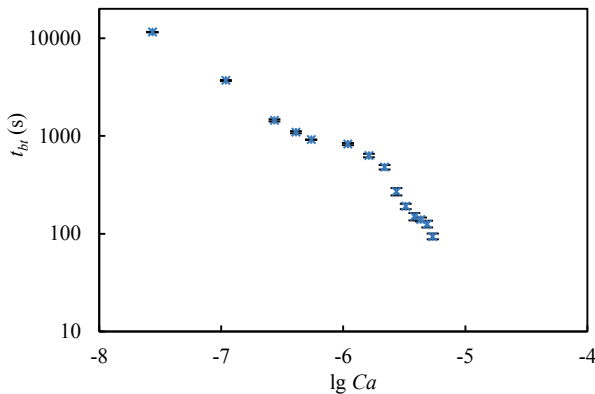
Figure 5 Breakthrough time at different capillary numbers. Error bars represent the standard deviation of three replicates for each Ca.

Figure 6 Total saturation versus dimensionless time for three different capillary numbers: (a) Ca=2,73E−8, (b) Ca=4,1E−7, (c) Ca=5,41E−6
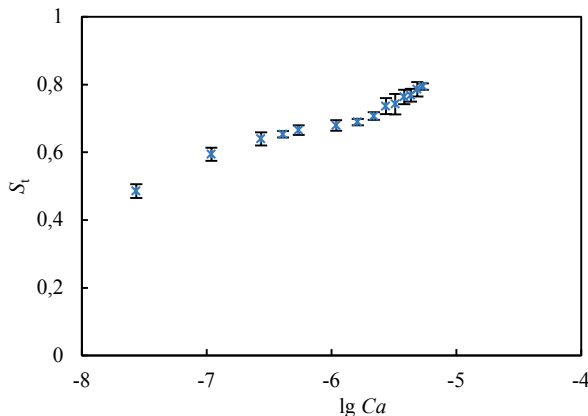

Figure 7 Total saturation of nonwetting phase at different capillary numbers. Error bars represent the standard deviation of three replicates for each Ca.

Approximately, similar local saturation profiles were obtained in the outlet region (column indexes larger than 1000) in all the experiments. The lowest drainage rate test showed the lowest S_x in most parts of the micromodel in the range of column indexes of 200 to 1000. This is an indication of high trapping and bypassing in this part. Obtained results showed the highest drainage efficiency at the entrance part of the micromodel in the column index of 200.

This can be attributed to the constant rate of boundary condition which forced the injected fluid to drain the water from different pore sizes due to local viscous force dominance in a high injection rate test.
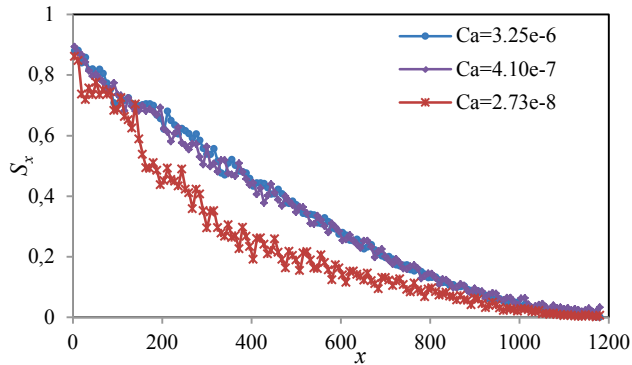
4.3 Fractal dimension

The surface and front fractal dimension of the test images are calculated using the box counting method as described before. The lower and upper length limits using fractal dimension calculations are considered respectively as the throat size and the width of the network respectively. Fig. 10 presents surface fractal dimension changes with dimensionless time for two different drainage rate tests: (a) Ca=2,73E−08 and (b) Ca=5,41E−06.
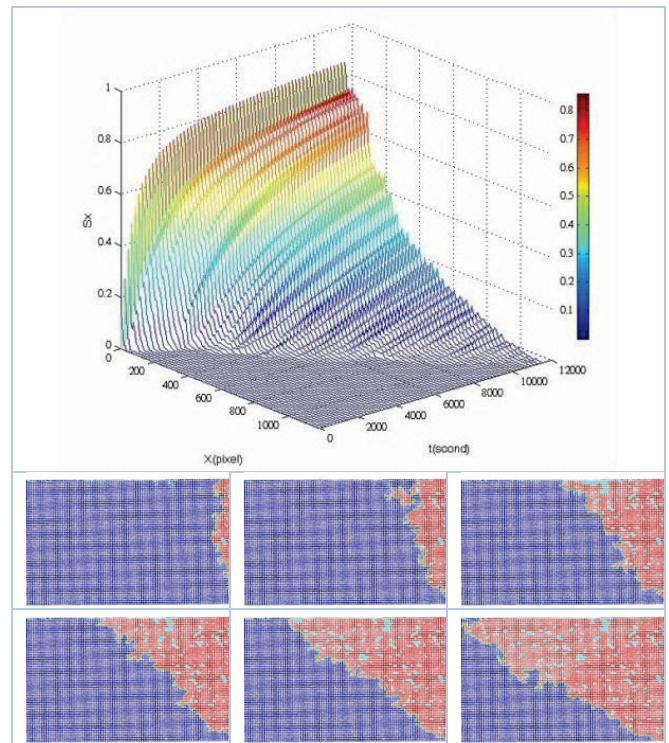

Figure 8 Local saturation with respect to time and position for Ca= 2,73E−8. (b) Flow pattern in different times before breakthrough.

Flow pattern structures at initial stages are similar for all capillary numbers which were reflected by close surface fractal dimensions in the figure. We can observe the same situation just before breakthrough time at which the displacement reached its steady state condition. Higher surface fractal dimensions corresponded to the flow patterns with lower trapping and bypassing structures. Therefore, high capillary number tests with higher microscopic displacement efficiencies show higher surface fractal dimensions as illustrated in Fig. 10.

Typical flow clusters for low and high injection rate tests, as presented in the figure, confirm the interrelationship of surface fractal dimension and developed displacement structure.

Figure 9 Saturation profile corresponding to the breakthrough time for three different capillary numbers (a) Ca=2,73E−8, (b) Ca=4,41E−7, (c) Ca=3,25E−6.
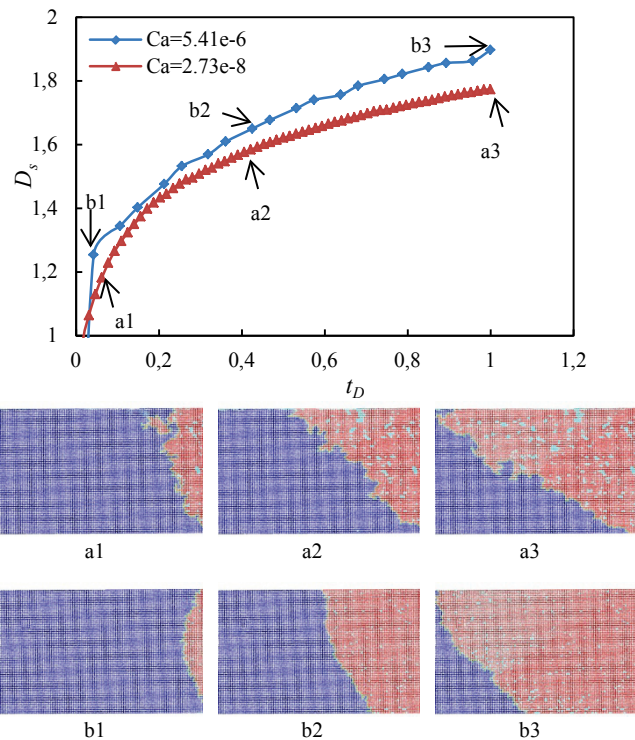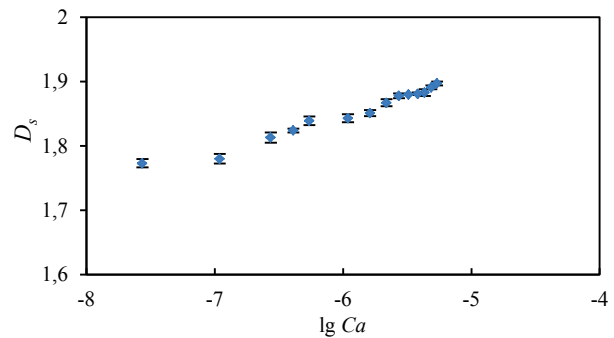

Figure 10 Evaluation of surface fractal dimension of invading phase with respect to time for two capillary numbers: (a) Ca=2,73E−8 (b) Ca=5,41E−6. Corresponding flow images are also shown, with indexes indicating associated data point.

As shown in Fig. 10, flow structure significantly changes with capillary number. For the test with Ca=2,73E−8 (subfigures: a1, a2, a3), the flow pattern exhibits capillary fingering characteristic and there are a number of trapped regions; while for the test with Ca=5,41E−6 (subfigures: b1, b2, b3) the flow shows compact pattern especially at late time. More trapping of the wetting phase occurs in the lower capillary number test.

Characteristic behaviour of surface fractal dimension at breakthrough time for all the conducted experiments is shown in Fig. 11. It should be noted that the dense generated clusters fully spread over the accessible network at high capillary number experiments lead to D_s

larger than 1,85. They can be considered as invasion percolation with trapping fractals in accordance with the fractal invasion classification provided by Lenormand et al. [14, 17]; Invasion percolation with trapping (IPT) is a flow type characterized with capillary force dominance i.e. when injection velocity is near zero. Inflows with low capillary numbers, viscous effects are negligible, and the pressures are thus uniform throughout each fluid. The pressure in the displacing fluid is, therefore, uniformly equal to the inlet pressure; while the pressure in the displaced fluid is uniformly equal to the outlet pressure. The pressure drop at the interface, which is equal to inlet pressure minus outlet pressure, is larger than the pressure required advancing the displacing fluid through the largest throat on the interface. This pressure drop must, therefore, always be positive, because the wetting fluid cannot displace the non-wetting fluid from an occupied pore-body. Therefore, a fully encircled region of wetting fluid is immobilized or trapped, in which the non-wetting fluid is prevented from advancing. It is worth noting that surface fractal dimension (D_s) eventually decreases as the capillary number is decreased and unstable structures were developed in low injection rate experiments.
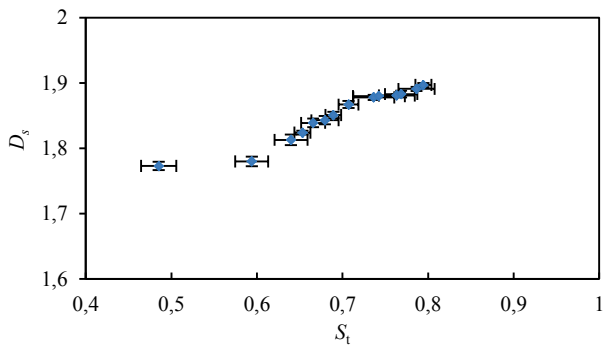

Figure 11 Surface Fractal dimension versus capillary number at breakthrough time. Error bars represent the standard deviation of three replicates for each Ca.

The average fractal dimension of all the experiments is D_s=1,85 (Fig. 12) which is higher than the fractal dimension of invasion percolation with trapping [34].
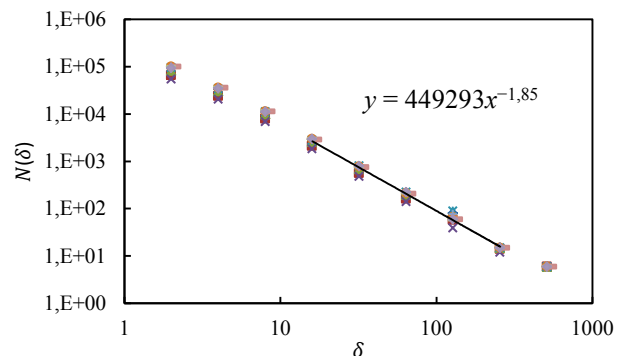

Figure 12 The data collapse from the box counting data for all the 14 experiments. The average fractal dimension obtained from the slope as D_s=1,85.

Both the S_t and D_s parameters follow an increasing trend with capillary number. In high injection rates with more compact clusters, both the S_t and D_s increases and vice versa. Therefore, a direct relationship between S_t and D_s is expected, as is demonstrated in Fig. 13.

Figure 13 Surface fractal dimension versus total saturation at breakthrough time for different capillary numbers. Error bars represent the standard deviation of three replicates for each Ca.

In addition to the surface fractal dimension, front fractal dimension D_f, also provides valuable information about displacement characteristics and structures. Front shape is a complicated function of mobility ratio, dominant forces and pore-level heterogeneities. In the conducted experiments, front region was extracted from the captured images and then analysed in detail for D_f calculation. As the front propagates, D_f calculation was repeated to arrest its progress pattern characteristics. D_f variations are presented in Fig. 14 for two drainage experiments up to their breakthrough time. In early times, when the nonwetting phase had not invaded all the pores of the entrance region, the front was not continuous and defining a fractal dimension is not even physically meaningful. When the invading fluid cluster was formed, D_f started to follow an increasing trend. Eventually, D_f approached a constant with local fluctuations around an average value which increased with capillary number. D_f showed more fluctuations in the low injection rate tests, which were originated from pore-level instabilities and local capillary fingering structures of the front. This behaviour became evident from inspection of displacement images during the process.
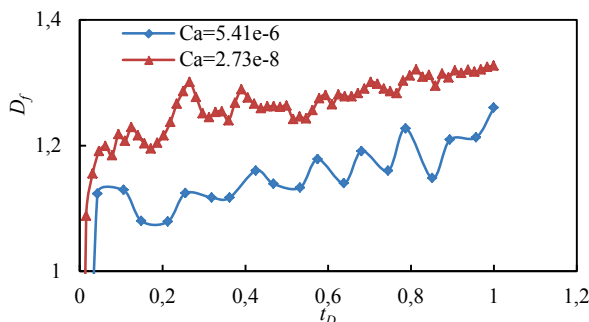

Figure 14 Evaluation of front fractal dimension of invading phase with respect to time for two capillary numbers until breakthrough time: (a) Ca=2,73E−8, (b) Ca=5,41E−6.

Front fractal dimensions at breakthrough time are shown in Fig. 15 for all the conducted tests. The average front fractal dimension of all the experiments was obtained as 1,32 (Fig. 16). This is close to the fractal dimension of the external perimeter of the invasion percolation cluster of D_e=4/3 [31, 38] and numerical simulation for viscosity matched fluid [40]. D_f followed a decreasing trend with capillary number which indicates a front change from an unstable fingering structure at slow drainage processes to a compact pattern at high injection

rates. This can be explained by the fact that trapping of the defending fluid in high capillary number decreases the effective mobility of displacing fluid and stabilizes the front.
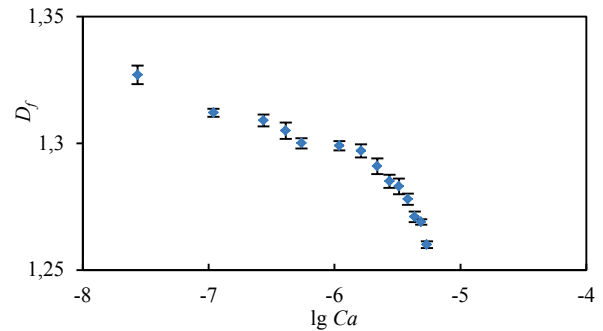
Figure 15 Front fractal dimension at breakthrough time for various capillary numbers. Error bars represent the standard deviation of three replicates for each Ca.
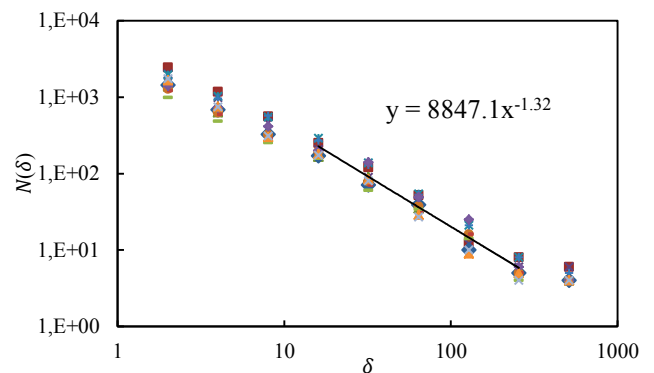
Figure 16 The data collapse from the box counting data for all the 14 experiments. The average fractal dimension obtained from the slope as D_f=1,32.

The above experimental studies and fractal analysis of the results showed a close relationship between the considered quantitative parameters and developed displacement patterns and structures. Therefore, it is possible to get a picture of the general displacement pattern and structures from fractal dimensional study of the front or the surface of invading fluid as described above.

4 Conclusion

Various drainage rates of viscosity matched fluids were conducted in a water-wet glass micromodel. Pore and throat size distributions of the model were very close in size to that of a typical real rock. The micromodel was fabricated with an advanced nanolithography technology. High resolution images of the tests were used to study the dynamic structure of the invading fluid. Displacements were performed in a wide range of capillary numbers between Ca=2,73E−8 and Ca=5,46E−6. Breakthrough time, total invading phase saturation S_t, local saturation S_x, surface fractal dimension D_s, and front fractal dimension D_f, were investigated for each experiment. Three parameters of breakthrough time S_t, and D_s are found to increase with increasing of the flow rate. This behaviour is the result of more stable structures and compact flow patterns which tend to develop in high capillary number experiments. This fact is also reflected in the decreasing

trend of D_f with capillary number which shows shorter front lengths appearing at higher rate tests. D_f also has a variable nature in each test starting from values less than one at early times, due to discontinuous sparse pore fillings, to somehow stabilized values larger than one at the later times. Local saturation curves are found to be comparable for different capillary number tests due to the same network pattern used in all the experiments. The average surface fractal dimension is found to be D_s=1,85, which is higher than the fractal dimension of invasion percolation with trapping. Moreover, the average front fractal dimension of D_f=1,32 is found to be in agreement with the fractal dimension of the external perimeter of the invasion percolation cluster. In other words, Two-phase flow patterns change from capillary fingering to compact flow as the capillary number is increased

The strong interrelationships between the considered parameters and the drainage patterns and structures are very lightening for proper displacement evaluation and planning in large scale field projects. More investigations are, however, required to explore the feature of unmatched viscosity displacements and other heterogeneous network patters with quantitative measures considered in this paper. Furthermore, capillary number is changed here only by changing the injection rates. It is worth to plan and run other series of tests with different viscosity and interfacial tension fluids to see how the displacement pattern varies with these properties at different values of capillary and viscous forces.

5 References

[1] Cottin, C.; Bodiguel, H.; Colin, A. Drainage in two-dimensional porous media: From capillary fingering to viscous flow. // Physical Review E. 82, 4(2010), pp. 3493-3505.

[2] Nittmann, J.; Daccord, G.; Stanley, H. E. Fractal growth of viscous fingers: quantitative characterization of a fluid instability phenomenon. // Nature. 314, 6007(1985), pp. 141-144.

[3] Ferer, M.; Bromhal, G. S.; Smith, D. H. Spatial distribution of avalanches in invasion percolation: their role in fingering. // Physica A: Statistical Mechanics and its Applications. 311, 1(2002), pp. 5-22.

[4] Mogensen, K.; Stenby, E. H. A dynamic two-phase pore-scale model of imbibition. // Transport in Porous Media. 32, 3(1998), pp. 299-327.

[5] Zhang, C.; Oostrom, M.; Wietsma, T. W.; Grate, J. W.; Warner, M. G. Influence of viscous and capillary forces on immiscible fluid displacement: Pore-scale experimental study in a water-wet micromodel demonstrating viscous and capillary fingering. // Energy & Fuels. 25, 8(2011), pp. 3493-3505.

[6] Ferer, M.; Ji, C.; Bromhal, G. S.; Cook, J.; Ahmadi, G.; Smith, D. H. Crossover from capillary fingering to viscous fingering for immiscible unstable flow: Experiment and modeling. // Physical Review E. 70, 1(2004), pp. 1-7.

[7] Willingham, T. W.; Werth, C. J.; Valocchi, A. J. Evaluation of the effects of porous media structure on mixing-controlled reactions using pore-scale modeling and micromodel experiments. // Environmental science & technology. 42, 9(2008), pp. 3185-3193.

[8] Er, V.; Babadagli, T.; Xu, Z. Pore-scale investigation of the matrix - fracture interaction during CO_2 injection in naturally fractured oil reservoirs. // Energy & Fuels. 24, 2(2009), pp. 1421-1430.

[9] Ferer, M.; Anna, S. L.; Tortora, P.; Kadambi, J. R.; Oliver, M.; Bromhal, G. S.; Smith, D. H. Two-phase flow in porous media: predicting its dependence on capillary number and viscosity ratio. // Transport in porous media. 86, 1(2011), pp. 243-259.

[10] Chang, L. C.; Tsai, J. P.; Shan, H. Y.; Chen, H. H. Experimental study on imbibition displacement mechanisms of two-phase fluid using micro model. // Environmental Earth Sciences. 59, 4(2009), pp. 901-911.

[11] Tsakiroglou, C. D.; Avraam, D. G.; Payatakes, A. C. Transient and steady-state relative permeabilities from two-phase flow experiments in planar pore networks. // Advances in water resources. 30, 9(2007), pp. 1981-1992.

[12] Lenormand, R.; Zarcone, C.; Sarr, A. Mechanisms of the displacement of one fluid by another in a network of capillary ducts. // J. Fluid Mech. 135, 34(1983), pp. 337-353.

[13] Ferer, M.; Sams, W. N.; Geisbrecht, R. A.; Smith, D. H. Fractal nature of viscous fingering in two-dimensional pore level models. // AIChE Journal. 41, 4(1995), pp. 749-763.

[14] Lenormand, R.; Zarcone, C. Invasion percolation in an etched network: measurement of a fractal dimension. // Physical review letters. 54, (1985), pp. 2226-2229.

[15] Birovljev, A.; Wagner, G.; Meakin, P.; Feder, J.; Jøssang, T. Migration and fragmentation of invasion percolation clusters in two-dimensional porous media. // Physical Review E. 51, 6(1995), pp. 5911-5915.

[16] Løvoll, G.; Méheust, Y.; Måløy, K. J.; Aker, E.; Schmittbuhl, J. Competition of gravity, capillary and viscous forces during drainage in a two-dimensional porous medium, a pore scale study. // Energy. 30, 6(2005), pp. 861-872.

[17] Lenormand, R.; Touboul, E.; Zarcone, C. Numerical models and experiments on immiscible displacements in porous media. // Journal of Fluid Mechanics. 189, 1(1988), pp. 165-187.

[18] Feder, J. Fractals. // Plenum Press, New York and London, (1988), pp. 14-74.

[19] Meakin, P. Fractals, scaling, and growth far from equilibrium. // Cambridge University Press, Cambridge. (1998).

[20] Sahimi, M.; Imdakm, A. O. The effect of morphological disorder on hydrodynamic dispersion in flow through porous media. // Journal of Physics A: Mathematical and General. 21, 19(1988), pp. 3833-3870.

[21] Wilkinson, D.; Willemsen, J. F. Invasion percolation: A new form of percolation theory. // J. Phys. A-Math. Gen. 16, 14(1983), pp. 3365-3376.

[22] Haines, W. B. Studies in the physical properties of soil. V. The hysteresis effect in capillary properties, and the modes of moisture distribution associated therewith. // The Journal of Agricultural Science. 20, 01(1930), pp. 97-116.

[23] Furuberg, L.; Feder, J. Dynamics of slow drainage in porous media. // Physical review letters. 68, 14(1992), pp. 2161-2164.

[24] Aker, E.; Måløy, K. J.; Hansen, A.; Basak, S. Burst dynamics during drainage displacements in porous media: Simulations and experiments. // EPL (Europhysics Letters). 51, 1(2000), pp. 55-61.

[25] Maslov, S. Time directed avalanches in invasion models. // Physical review letters. 74, 4(1995), pp. 562-565.

[26] Furuberg, L.; Måløy, K. J.; Feder, J. Intermittent behavior in slow drainage. // Physical Review E. 53, 1(1996), pp. 966-977.

[27] Babadagli, T. Invasion percolation in correlated porous media. // Physica A: Statistical Mechanics and its Applications. 285, 3(2000), pp. 248-258.

[28] Blunt, M. J. Flow in porous media—pore-network models and multiphase flow. // Current opinion in colloid & interface science. 6, 3(2001), pp. 197-207.

[29] Sahimi, M.; Hashemi, M.; Ghassemzadeh, J. Site-bond invasion percolation with fluid trapping. // Physica A: Statistical Mechanics and its Applications. 260, 3(1998), pp. 231-243.

[30] Lee, S. B. Invasion percolation between two sites in two, three, and four dimensions. // Physica A: Statistical Mechanics and its Applications. 388, 12(2009), pp. 2271-2277.

[31] Grossman, T.; Aharony, A. Structure and perimeters of percolation clusters. // Journal of Physics A: Mathematical and General. 19, 12(1986), pp. 745-751.

[32] Grossman, T.; Aharony, A. Accessible external perimeters of percolation clusters. // Journal of Physics A: Mathematical and General. 20, 17(1987), pp. 1193-1201.

[33] Frette, O. I.; Maløy, K. J.; Schmittbuhl, J.; Hansen, A. Immiscible displacement of viscosity-matched fluids in two-dimensional porous media. // Physical Review E. 55, 3(1997), pp. 2969-2974.

[34] Ferer, M.; S Bromhal, G.; Smith, H. D. Fractal dimension and avalanches of invasion percolation: the effect of aspect ratio. // Physica A: Statistical Mechanics and its Applications. 334, 1(2004), pp. 22-38.

[35] Man, H. N.; Jing, X. D. Pore network modelling of electrical resistivity and capillary pressure characteristics. // Transport in Porous Media. 41, 3(2000), pp. 263-285.

[36] Stauffer, D.; Aharony, A. Introduction to percolation theory, CRC press, 1994.

[37] Sheppard, A. P.; Knackstedt, M. A.; Pinczewski, W. V.; Sahimi, M. Invasion percolation: new algorithms and universality classes. // Journal of Physics A: Mathematical and General. 32, 49(1999), pp. 521-529

[38] Meakin, P. Invasion percolation on substrates with correlated disorder. // Physica A: Statistical Mechanics and its Applications. 173, 3(1991), pp. 305-324.

[39] Dias, M. M.; Wilkinson, D. Percolation with trapping. // Journal of Physics A: Mathematical and General. 19, 15(1986), pp. 3131-3146.

[40] Hou, J.; Li, Z. Q.; Zhang, S. K.; Cao, X. L.; Du, Q. J.; Song, X. W. Computerized tomography study of the microscopic flow mechanism of polymer flooding. // TranspPorous Med. 79, 3(2009), pp. 407-418.

[41] Yan, J.; Luo, X.; Wang, W.; Toussaint, R.; Schmittbuhl, J.; Vasseur, G.; Chen, F.; Yu, A.; Zhang, L. An experimental study of oil secondary migration in a three dimensional porous space. // AAPG Bulletin. 96, 5(2012), pp. 773-788.

[42] Nsir, K.; Schäfer, G.; Di Chiara Roupert, R.; Razakarisoa, O.; Toussaint, R. Laboratory experiments on DNAPL gravity fingering in water-saturated porous media. // Internat. J. Multiphase Flow. 40(2012), pp. 83-92.

[43] Aker, E.; Måløy, K. J.; Hansen, A.; Batrouni, G. G. A two-dimensional network simulator for two-phase flow in porous media. // Transport in Porous Media. 32, 2(1998), pp. 163-186.

[44] Morin, N. Hands-on demonstration of basic processing. // Nano-Fab, University of Alberta, Edmonton, Alberta, Canada, 2001.

[45] Tai, K. Nano-Fab glass microfluidic device fabrication manual. // Nano-Fab, University of Alberta, Edmonton, Alberta, Canada, 2005.

Authors' addresses

Mohammad Nadafpour
Institute of Petroleum Engineering, School of Chemical Engineering, College of Engineering, University of Tehran, Tehran, Iran
E-mail: m_nadafpour@ut.ac.ir

Mohammad Reza Rasaei (Corresponding Author)
Institute of Petroleum Engineering, School of Chemical Engineering, College of Engineering, University of Tehran, Tehran, Iran
Tel: +98-2161114746
E-mail: mrasaei@ut.ac.ir